Transfer of CVD-Grown Monolayer Graphene onto Arbitrary Substrates

Ji Won Suk,[†,‡] Alexander Kitt,[§] Carl W. Magnuson,[†] Yufeng Hao,[†] Samir Ahmed,[§] Jinho An,[†] Anna K. Swan,[§] Bennett B. Goldberg,[§] and Rodney S. Ruoff[†,‡,*]

[†]Department of Mechanical Engineering and the Materials Science and Engineering Program, The University of Texas at Austin, Austin, Texas 78712, United States, [‡]DARPA Center for Integrated Micro/Nano-Electromechanical Transducers (iMINT), United States, and [§]Departments of Physics and Electrical and Computer Engineering, Photonics Center, and Center for Nanoscience and Nanobiotechnology, Boston University, Boston, Massachusetts 02215, United States

Graphene, studied since the 1960s as monolayer graphite on metal substrates[1–5] and earlier still as individual layers in graphite intercalation compounds, warrants its current interest due to its exciting properties.[5–7] The first electrical measurements of single-layer graphene were published in 2004,[8] followed by other studies involving fabrication of isolated samples by mechanical exfoliation of graphite in 2005.[6,9] However, mechanical exfoliation[10–12] is a time-consuming process that yields relatively small samples. Thus, mechanical exfoliation cannot address the need for mass fabrication of large-area uniform monolayer graphene. Chemical vapor deposition (CVD) has been shown to provide large area coverage. Few-layer graphene was first grown on Ni foils,[13] and shortly thereafter self-limited growth of single-layer graphene on copper foils was demonstrated.[14] It has been shown that single-crystal, large-area (~0.5 mm on a side) uniform monolayer graphene can be controllably grown on copper foils.[15]

Reliable transfer of large-area monolayer graphene onto arbitrary substrates is a critical step in the use of CVD-grown graphene for most practical applications. Since poly(methyl methacrylate) (PMMA) has been used as a carrier material for transferring carbon nanotubes[16] and mechanically exfoliated graphene flakes,[17,18] it has also been widely used to transfer CVD-grown graphene to target substrates.[14,19] In a recent study, a modified PMMA transfer technique using a second, liquid PMMA coating step exhibited enhanced performance of transparent conductive electrodes made of CVD-grown graphene films.[20] The improved transfer provided a sheet resistance of 2.1 kΩ/sq for monolayer graphene films with a transmittance of 97.4%. Although an improvement over previous transfer techniques, the sheet resistance is still much larger than the intrinsic graphene sheet resistance of ~30 Ω/sq.[21] Furthermore, this technique can be used only to transfer graphene onto flat substrates.

Suspending graphene membranes over perforated substrates eliminates substrate interactions and has allowed various kinds of fundamental studies including transmission electron microscopy (TEM),[22–26] thermal transport,[27,28] mechanical,[29] and optical measurements.[30] Several methods have been developed to make suspended membranes from CVD-grown monolayer graphene over holes. The copper foil was directly etched lithographically,[23] or the graphene/copper was directly attached and transferred to flexible thin carbon films with holes to minimize contamination of graphene.[24,31] However, these methods

ABSTRACT Reproducible dry and wet transfer techniques were developed to improve the transfer of large-area monolayer graphene grown on copper foils by chemical vapor deposition (CVD). The techniques reported here allow transfer onto three different classes of substrates: substrates covered with shallow depressions, perforated substrates, and flat substrates. A novel dry transfer technique was used to make graphene-sealed microchambers without trapping liquid inside. The dry transfer technique utilizes a polydimethylsiloxane frame that attaches to the poly(methyl methacrylate) spun over the graphene film, and the monolayer graphene was transferred onto shallow depressions with 300 nm depth. The improved wet transfer onto perforated substrates with 2.7 μm diameter holes yields 98% coverage of holes covered with continuous films, allowing the ready use of Raman spectroscopy and transmission electron microscopy to study the intrinsic properties of CVD-grown monolayer graphene. Additionally, monolayer graphene transferred onto flat substrates has fewer cracks and tears, as well as lower sheet resistance than previous transfer techniques. Monolayer graphene films transferred onto glass had a sheet resistance of ~980 Ω/sq and a transmittance of 97.6%. These transfer techniques open up possibilities for the fabrication of various graphene devices with unique configurations and enhanced performance.

KEYWORDS: graphene · transfer · membranes · transparent conductive films · Raman spectroscopy
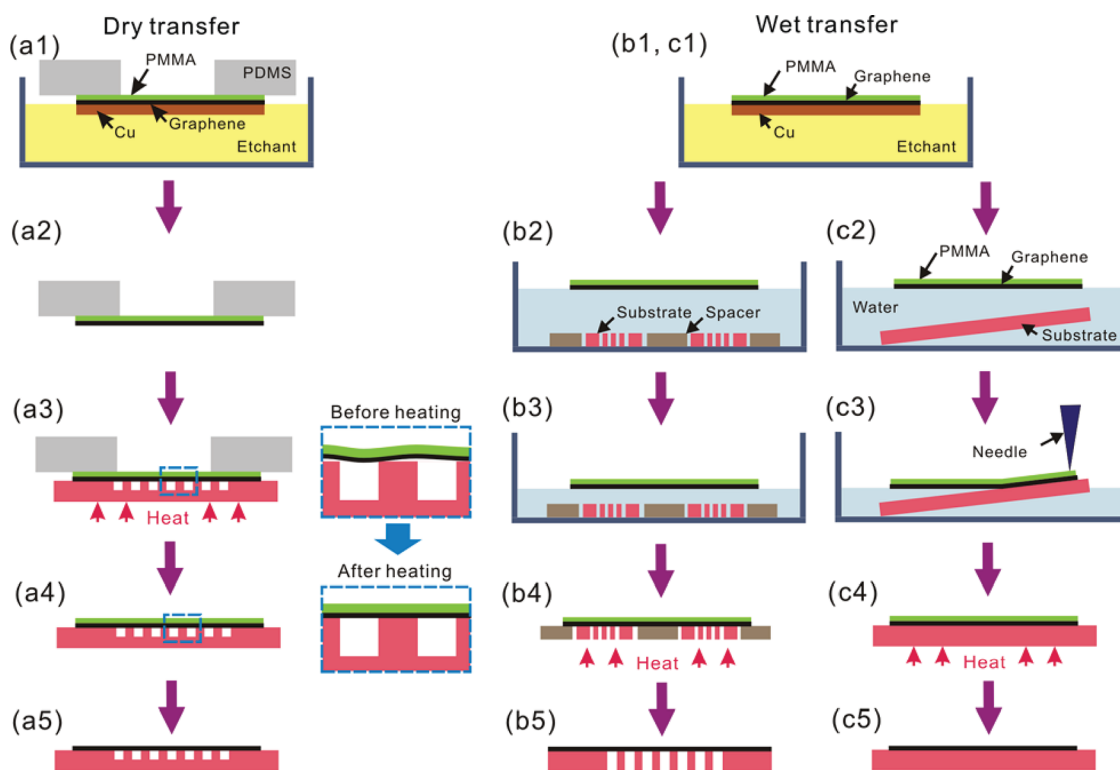
© 2011 American Chemical Society

Figure 1. Schematic illustration of dry and wet transfer processes. (a) Dry transfer onto shallow depressions. Wet transfer onto (b) perforated substrates and (c) flat substrates. The boxes with dashed lines in (a3) and (a4) show magnified views.

require specialized fabrication processes and cannot be used for rigid substrates due to the roughness and rigidity of graphene/copper foils.

Mechanically exfoliated graphene membranes that seal depressed wells or chambers have been used to demonstrate the impermeability of graphene membranes[32] and for nanoindentation tests.[33] This kind of graphene-sealed microchambers provides a unique separation barrier between two different environments, which can be used for compliant membrane sensors that detect pressure, chemical/biological reactions, and other changes.[32,34] Transfer of CVD graphene onto these substrates is particularly challenging since a dry transfer technique is required to avoid trapping transfer or etchant liquids in the wells. Dry transfer techniques have been developed to peel off multilayer graphene grown on SiC substrates by using a bilayer film of gold/polyimide,[35] a thermal release tape,[36] or an electrostatic process.[37] However, these techniques were applied for flat substrates with epitaxially grown multilayer graphene. To date, a dry transfer technique for CVD-grown monolayer graphene over patterned substrates has not yet been developed.

In this report, we present a novel dry transfer technique for transfer of CVD-grown monolayer graphene onto shallow wells. A polydimethylsiloxane (PDMS) frame is used to support the graphene/PMMA film, allowing it to be removed from the copper etchant and dried. A PMMA heat treatment step is used following the graphene transfer to increase the adhesion between the graphene

and the substrate. Copper foils used in CVD have an irregular surface that is further roughened due to surface reconstruction during the high-temperature anneal and growth. Graphene follows the surface morphology of the underlying copper during the growth process, making the adhesion of transfer materials to the graphene films a challenging process. After removing the copper foil, the transferred graphene supported by its polymer does not lie flat on the substrate. Small gaps form between the graphene and the substrate. The incomplete contact of graphene with the substrate causes cracks and tears when the polymer material is removed. Here, we overcome this problem by softening the transfer layer (PMMA) with heat treatment. When the PMMA is heated above the glass transition temperature (T_g), it softens and becomes more flexible. The gap between the graphene and the substrate are reduced, increasing the adhesion as the transfer layer molds to the substrate. When used in a gentle wet transfer process, the heat treatment step increases the quality of transfer onto flat and perforated substrates. Raman spectroscopy and TEM of graphene suspended over the holes show the intrinsic characteristics of graphene. Graphene transferred onto flat substrates using the heat treatment has lower sheet resistance than graphene transferred using other techniques.

RESULTS AND DISCUSSION

Figure 1 shows the schematic illustration of the dry and wet transfer processes for the three substrate types: shallow wells, perforated substrates, and flat

substrates. Transferring graphene onto closed wells is more difficult than onto flat or perforated substrates because of the possibility of trapping liquid in the wells. The liquid etching of copper to free the CVD graphene is currently unavoidable, which necessitates the drying of graphene prior to transfer. Without support, the graphene layer is too flimsy to remove from the etchant without wrinkling or otherwise destroying the membrane. In our approach, PDMS acts as a flexible frame to hold the PMMA/graphene film, enabling the film to be removed from the etchant, dried, placed on the target substrate, and heat treated. PDMS has been widely used as a carrier or supporting material for graphene or graphene oxide films due to its flexibility, robustness, adhesion to samples, and transparency.[19,38−40] First, relatively thick PMMA was coated on a graphene/copper foil. A PDMS block with a through hole in the center is attached to the PMMA/graphene/copper films by natural adhesion. The copper is then etched while the PDMS/PMMA/graphene block is floated over the solution (Figure 1(a1)). Using the PDMS "handle", the composite is easily rinsed and dried after etching (Figure 1(a2)), thereby removing the liquid used in the etching process. Next, the PDMS/PMMA/graphene composite is placed onto the target substrate, covering the wells. The substrate is heated above the T_g of PMMA (Figure 1(a3)). The heat treatment allows the wavy and rough PMMA/graphene film to make full contact with the target substrate, as shown in the magnified views of Figure 1(a3, a4). After heating, the adhesion of the graphene to the substrate is strong enough to peel off the PDMS block without delaminating the PMMA/graphene film (Figure 1(a4)). Finally, the PMMA is thermally removed in a furnace at 350 °C with Ar and H_2 for ∼2 h, without the use of any solvent. The end result is a reproducible dry transfer technique.

The dry transfer was demonstrated with patterned wells of two different depths: 2 μm and 300 nm. Figure 2(a) shows a scanning electron microscopy (SEM) image of graphene suspended over deep wells. If a membrane is broken, the well has a white ring around its edge in the SEM image due to the charging of the exposed SiO_2 layer by the electron beam. Figure 2(b) shows a SEM image of a suspended membrane over a 5.1 μm diameter well. Note that the wrinkle spanning the well is straight. This indicates that the membrane has not been drawn into the well. For this deep well, a ∼1.5 μm thick PMMA layer was used for transfer and the sample was heated at 180 °C for >3 h in air before PMMA removal. However, these conditions did not give good coverage of suspended membranes over the shallow wells. The heat treatment of the relatively thin PMMA film caused the PMMA/graphene films to collapse to the bottom of the majority of the shallow wells. Relatively thick PMMA (∼2.7 μm thickness) and a lower temperature treatment (150 °C) was used to
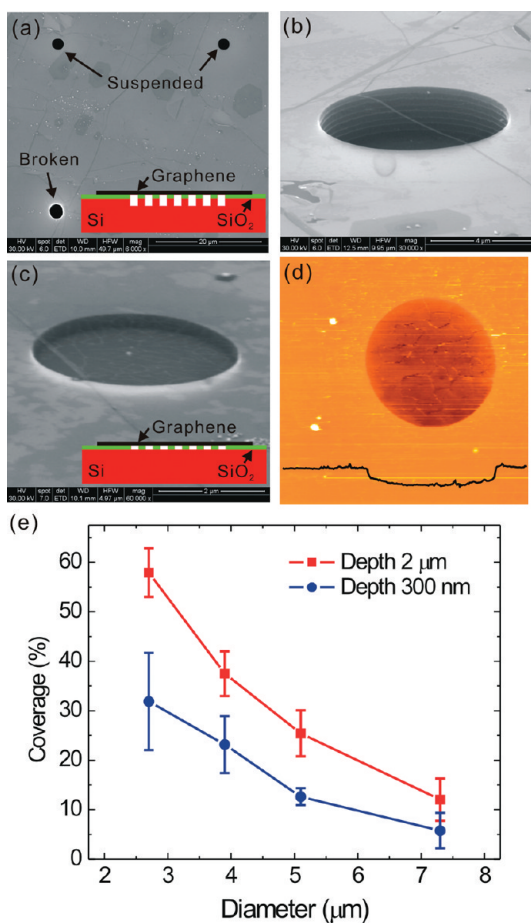

Figure 2. Monolayer graphene transferred onto wells. (a, b) SEM images of graphene membranes over 2 μm deep wells with 2.7 and 5.1 μm diameter, respectively. The broken membrane has a white ring around its edge due to charging of the substrate in SEM. (c) SEM image of a graphene membrane over a 300 nm deep well with 3.9 μm diameter. (a and c insets) Schematics of samples. (d) AFM topology image (10 μm × 10 μm) of a graphene membrane over a 300 nm deep well with 5.1 μm diameter. The black line represents the line profile along the center of the membrane. (e) Coverage of suspended graphene membranes over different sizes of wells.

increase the rigidity of the film and thus minimize the contact of the film to the bottom of wells. At temperatures closer to T_g (125 °C) of the PMMA, the PMMA needs more time to relax and make full contact with the substrate. When treated for <3 h, we found there was not sufficient adhesion. When heated for >12 h at 150 °C, the PMMA/graphene film adhered well to the substrate when the PDMS block was peeled off. Figure 2(c) shows a SEM image of a suspended membrane over a 3.9 μm diameter well with 300 nm depth. The visible, undistorted wrinkle in the graphene sheet passing through the well indicates that the membrane was suspended. An atomic force microscopy (AFM) topology image confirmed that the membrane was completely suspended over the shallow well (Figure 2(d)). Presumably due to van der Waals attraction of the graphene to the walls and the flexibility of
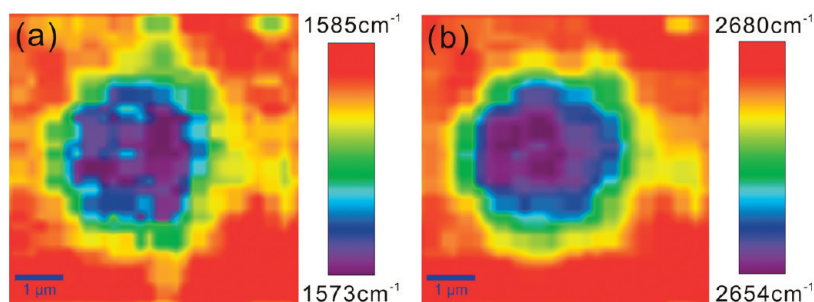
Figure 3. Spatial Raman maps of (a) G- and (b) 2D-band energies for graphene covering a 300 nm deep well.

the PMMA film during heat treatment, the graphene membrane adheres to the sidewall of the well for a few nanometers. Figure 2(e) shows the percentage of covered membranes as a function of the diameter of the wells. Even though this process has not yet been fully optimized, the percentage of covered holes was relatively high. For 2.7 μm diameter holes, 59% of the 2 μm deep holes and 32% of the 300 nm deep holes were covered. As expected, the coverage of suspended membranes decreases as the diameter of the wells increases. Nonetheless, using this technique we could achieve large graphene membranes with up to 10.5 and 7.3 μm diameters for 2 μm and 300 nm deep wells, respectively.

Figure 3 shows Raman maps of the G- and 2D-band peak positions of monolayer graphene transferred onto a shallow 3.9 μm diameter well. The large downshift of both the G- and 2D-bands is consistent with biaxial strain that develops when the graphene membrane adheres to the side wall. On the basis of previously measured shift rates,[41] a G-band shift of $\sim$12 cm^{-1} indicates 0.16 $\pm$ 0.01% strain, while a 2D shift of $\sim$26 cm^{-1} indicates 0.13 $\pm$ 0.01% strain. This level of strain can be explained by the graphene adhering to the side walls for 3 nm and is consistent with the AFM data, which show a few nanometers of side wall adhesion.

The PMMA heat treatment step can also be used to improve the quality of graphene that is wet-transferred to flat or perforated substrates. For flat samples, a thin PMMA film ($\sim$100 nm thick) is spin-coated onto the graphene grown on copper foil. The copper foil is etched away, and the PMMA/graphene film rinsed with distilled water (Figure 1(c1)). The target substrate is placed in the water at an inclined angle (Figure 1(c2)), and the PMMA/graphene film is lowered onto the substrate by removing water with a syringe (Figure 1(c3)). A needle is useful for positioning the film on the substrate. The substrate is inclined to help the PMMA/graphene film spread across the substrate from one side as the water level is lowered. This gentle process reduces the tearing of the PMMA/graphene films. The drying process slightly stretches and flattens the graphene. Finally, the dried PMMA/graphene/substrate is heated above the T_g of the PMMA, but below

the melting temperature (Figure 1(c4)), as was done in the dry transfer, and the PMMA is removed with acetone.

The transfer process of graphene onto perforated substrates is complicated by the potential for freestanding graphene to be broken by surface tension during drying. A TEM grid having 10 000 holes (2.7 μm diameter) in a 200 nm thick silicon nitride film was used to demonstrate the transfer of graphene onto perforated substrates. Ammonium persulfate was used to etch the copper foil. The ammonium persulfate provides a cleaner graphene surface than iron(III) nitrate, possibly because iron(III) nitrate leaves some iron oxide contamination.[23] Since the target substrate is only 3 mm in diameter, the much larger PMMA/graphene membrane can bow around the substrate. To ensure full, even contact between the graphene and substrate, multiple target substrates with spacers in between were used so that the graphene/PMMA membrane was fully supported (Figure 1(b2)). To avoid rupturing the suspended graphene with surface tension, critical point drying is usually used.[22,42] As a less time-consuming alternative, hexamethyldisilazane (HMDS) was used as a dehydrating solution. For this size of membranes, its rapid evaporation and low surface tension prevent the membranes from breaking.[43]

This process covers a high percentage of holes with high-quality graphene. Among 10 000 holes, only 2% of the holes had voids after the transfer, as shown in Figure 4(a). The broken holes appear dark in the SEM (Figure 4(b)). The removal of PMMA using acetone left a residue of polymer on the graphene film. Further cleaning was necessary in order to observe the atomic structure of graphene.[44] The transferred graphene was annealed at 400 °C with Ar and H$_2$ for $\sim$1 h. 94% of 10 000 holes survived thermal cycling. Figure 4(c) shows a high-resolution TEM image in which relatively clean graphene areas longer than 30 nm in length can be seen. A selected area electron diffraction (SAED) pattern obtained in TEM shows the hexagonal pattern of monolayer graphene (Figure 4(c) inset). This transfer technique also works for transfer onto larger holes. Figure 4(d) shows graphene membranes transferred onto $\sim$10 μm diameter holes created by deep silicon
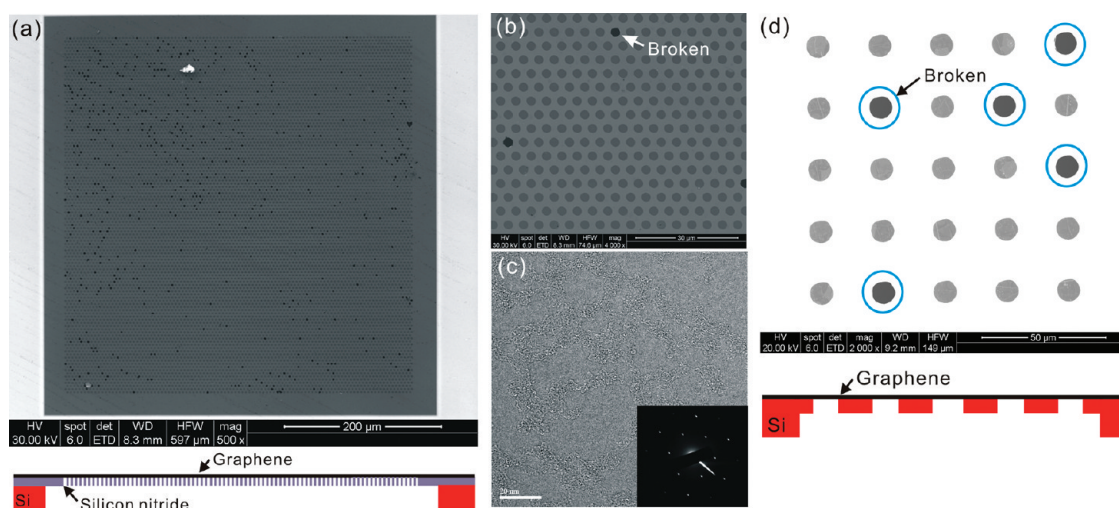
Figure 4. SEM and TEM images of monolayer graphene transferred onto perforated substrates. (a) Low- and (b) high-magnification SEM images of graphene on perforated silicon nitride supporting film having 2.7 μm diameter holes. A schematic of the sample is shown below (a). The dark holes indicate broken membranes. (c) High-resolution TEM image of graphene suspended over a hole in the silicon nitride TEM grid. The inset shows a SAED pattern that is consistent with monolayer graphene. (d) SEM image of monolayer graphene on a silicon substrate having $\sim$10 μm diameter holes with a schematic of the sample. Five dark holes (blue circles) are broken membranes, and the remaining 20 membranes are suspended.

etching. For a membrane this large, direct removal of the PMMA by annealing at high temperature was used. Twenty of the 25 membranes in Figure 4(d) survived the process. Earlier work has shown that graphene membranes can be transferred by thermally decomposing the PMMA film at 300−350 °C in air for 2−4 h.[26,45] However, oxygen in air can damage the graphene. When identically grown and transferred graphene has its PMMA removed by heating in atmosphere, we observed a Raman D peak that was roughly as high as the G peak, indicating much greater disorder than when the PMMA is removed by heating in an Ar/H$_2$ environment.

Raman spectroscopy was used to evaluate the quality of the suspended CVD-grown graphene. Figure 5(a−c) shows Raman spectra (514 nm laser wavelength) of CVD-grown monolayer graphene transferred onto SiO$_2$/Si and suspended graphene on a silicon nitride TEM grid. The optical power was 250 μW, low enough to avoid heating. The G and 2D peaks of monolayer graphene supported on SiO$_2$/Si are positioned at $\sim$1588 and $\sim$2690 cm^{-1}, respectively. The suspended graphene on the silicon nitride grid shows peaks that are downshifted to $\sim$1584 cm^{-1} (G) and $\sim$2685 cm^{-1} (2D). A small D peak, indicative of defects, is visible at $\sim$1350 cm^{-1}. The D peak does not increase in strength for the suspended sample, indicating that no additional cracks or tears exist across the sampled suspended areas. Table 1 shows the Raman characteristics for the suspended graphene membranes. The intensity ratio of D to G, I_D/I_G, varies between 0.06 and 0.12, and the 2D to G intensity ratio, I_{2D}/I_G, varies between 8 and 11, significantly higher than for the graphene on the SiO$_2$/Si surface, $I_{2D}/I_G \approx 5.4$.
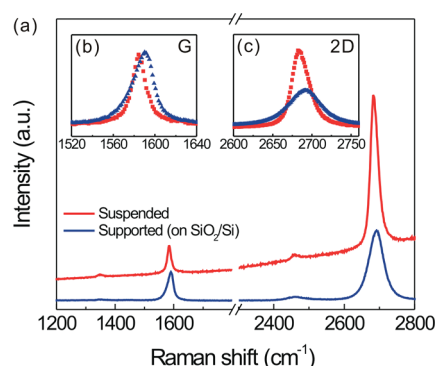

Figure 5. (a) Raman spectra of monolayer graphene on flat SiO$_2$/Si and perforated silicon nitride supporting film using a 514 nm wavelength laser. (b) Raman spectra of G-band region (1520−1640 cm^{-1}). (c) Raman spectra of 2D-band region (2600−2750 cm^{-1}).

TABLE 1. Raman Characteristics of Suspended Graphene Membranes

	G-band		2D-band			
membrane	ω (cm^{-1})	fwhm (cm^{-1})	ω (cm^{-1})	fwhm (cm^{-1})	I_D/I_G	I_{2D}/I_G
1	1585.0	15.8	2684.8	23.7	0.082	11.03
2	1583.9	15.1	2683.0	22.7	0.064	9.30
3	1585.0	15.8	2686.0	23.7	0.186	7.99
4	1584.7	15.5	2685.1	23.8	0.121	8.67

We use the measured Raman data to evaluate the degree of doping and strain in the suspended sample. Full width at half-maximum (fwhm) and frequencies (ω) of the G- and 2D-bands are sensitive to doping,[46−49] strain,[41,50] and temperature.[27,28,51,52] We rule out heating effects since a decrease in power by a factor of
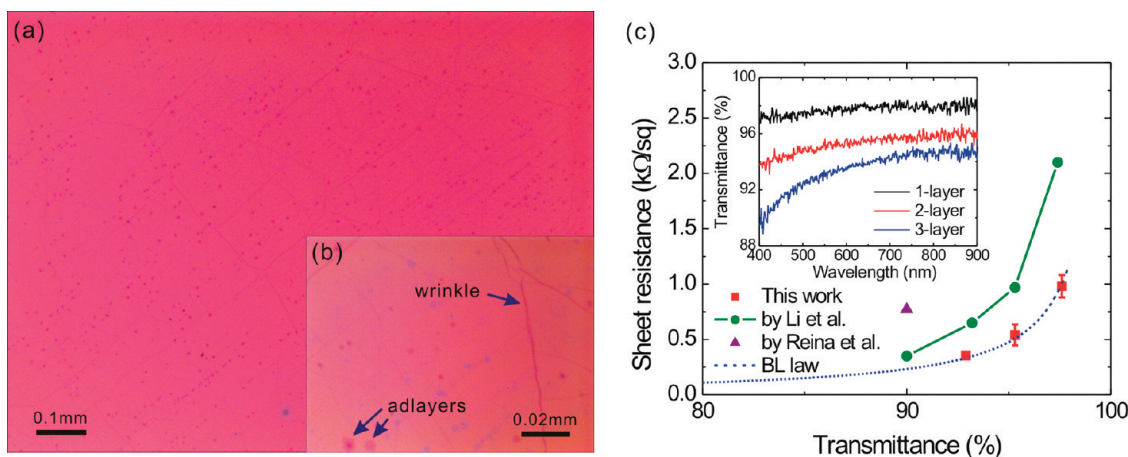
Figure 6. Evaluation of graphene films transferred onto flat substrates. (a, b) Optical images of large-area monolayer graphene transferred onto 285 nm SiO$_2$: (a) field of view 1.2 mm × 0.9 mm and (b) field of view 0.12 mm × 0.09 mm. (c) Sheet resistance as a function of transmittance at λ = 550 nm. The squares are the results from graphene transferred to glass slides by this method. The circle and triangle represent CVD-grown graphene grown on copper by Li *et al.*[20] and nickel by Reina *et al.*,[58] respectively. The blue dotted line represents the Beer−Lambert law (indicated as "BL law") fitted to results from this work. The inset is the transmittance of our *n*-layer graphene films as a function of wavelength of the incident light with a blank coverslip used for background subtraction.

~6 caused a G-band downshift by only a small amount, <0.1 cm^{-1}. On the basis of previously measured temperature shift rates,[52] this shift corresponds to heating by less than 10 °C. We use the G and 2D peak positions to analyze the strain and doping level. Due to the circular geometry, there is no preferential strain direction, and we assume uniform biaxial strain. Previous measurements show that the 2D-band shifts by less than 1 cm^{-1} for carrier concentrations below 3×10^{12} cm^{-2},[49] but has a large strain dependence, shifting by 203 cm^{-1}/% for biaxial strain.[41] Hence, we use the 2D peak position to evaluate the strain. For a 514 nm excitation, the unstrained 2D feature is expected to be at 2683 cm^{-1}, compared to 2683−2685 cm^{-1} on the measured suspended samples.[53] Thus, the measured frequencies correspond to strains of less than 0.01%. Having eliminated temperature and strain effects, the G peak position and width are only a function of doping. With increased electron or hole doping, the G-band frequency shifts up and the width decreases.[46−49] Comparing the large measured G widths and low measured frequencies to theoretical results,[46] we estimate doping levels less than 1×10^{12} cm^{-2}, consistent with the increase of the integrated 2D to G intensity ratio described above.[54,55] We also note that the increase of the integrated intensity ratio of the 2D-band to the G-band, I_{2D}/I_G, from 5.4 to 9.0 upon suspension is partially due to the etalon effect in the 285 nm thick SiO$_2$ cavity, which accounts for a calculated 22% of the ~66% increase. The remaining increase, having eliminated strain and temperature effects, is another indicator that the doping is decreased when the graphene is decoupled from the substrate. Hence, the spectrum from the suspended graphene demonstrates near-intrinsic properties of the graphene with doping less than 1×10^{12} cm^{-2}, strain less than 0.01%, and low disorder.

The improved transfer resulted in fewer cracks and tears in graphene films transferred onto flat substrates. Figure 6(a) shows an optical image of monolayer graphene transferred onto a 285 nm thick SiO$_2$ substrate at low magnification (1.2 mm × 0.9 mm). We could not locate any major cracks or tears. Figure 6(b) is a high-magnification optical image (0.12 mm × 0.09 mm), which shows typical features of CVD-grown graphene, namely, wrinkles and adlayers. These results reproducibly showed a significantly reduced density of cracks and tears on transferred graphene films and improved the electrical quality of the CVD graphene films. Monolayer graphene with ~1 × 1 cm^2 area was transferred onto a glass coverslip. Figure 6(c) shows the sheet resistance as a function of the optical transmittance. The transmittance was varied by stacking monolayer graphene sequentially, thereby making bilayer and trilayer graphene films. Monolayer graphene was measured to have a sheet resistance of ~980 Ω/sq with a transmittance of 97.6%. The sheet resistances for bilayer and trilayer graphene films were ~540 and ~350 Ω/sq with transmittance of 95.3% and 92.9%, respectively. The relationship between sheet resistance and transmittance generally follows the Beer−Lambert law.[56] According to the Beer−Lambert law, the transmittance of light (*T*) through a homogeneous material is $T = e^{-\alpha d}$, where *d* is the film thickness, α is the effective absorption coefficient given by $\alpha = 4\pi k/\lambda$, *k* is the extinction coefficient, and λ is the wavelength of incident light. The sheet resistance is defined as $R = 1/Gd$, where *G* is the material conductivity. Combining these two equations yields

$$R = \frac{-4\pi k}{G\lambda \ln T} \qquad (1)$$

where *k* is ~1.4 for graphene at 550 nm wavelength.[57] The electrical conductivity of a 2D material can be calculated from $\sigma = ne\mu$, where *n* is the carrier density, *e* the

elementary charge, and μ the mobility. By fitting the experimental sheet resistance and transmittance with eq 1 (the dotted line in Figure 6(c)), the electrical conductivity of our graphene films was found to be $\sim 3.0 \times 10^6$ S/m. While a direct calculation of our mobility is not possible due to the unknown doping level, we can calculate a lower bound. The measured G position and width establish an upper level of $n = 4 \times 10^{12}$ cm^{-2}, which corresponds to a lower limit of the mobility of 1.5×10^3 cm^2 V^{-1} s^{-1}. This lower limit is 2 orders of magnitude below the intrinsic limit of mobility at room temperature.[21] This could be due to an overestimation of n, impurity scattering by the substrate (SiO$_2$), small cracks formed during the transfer process, other imperfections in the graphene films such as grain boundaries, defects, and wrinkles, or any combination of these. Yet, compared to the previously reported results,[20,58] our method significantly enhanced the electrical conductivity of transferred graphene films. Particularly, when comparing graphene films having the same quality (grown at the same time) that were transferred using the second liquid PMMA coating method by Li *et al.*[20] and our method, the sheet resistance obtained from our transfer technique was more than a factor of 2 lower.

CONCLUSION

A novel dry transfer technique was developed that allows CVD graphene to be transferred over microchambers for the first time. This technique can be used to fabricate a number of devices that rely on the unique separation layer between the two different environments. The novel dry transfer technique uses a PDMS frame attached to the PMMA/graphene films to controllably remove the graphene from the etchant along with a heat treatment step to increase the adhesion between the graphene and the substrate. The heat treatment step can also be used in wet transfers to increase the quality of graphene transferred to flat and perforated substrates. Graphene suspended over perforated holes allowed us to measure the intrinsic nature of CVD-grown graphene using Raman spectroscopy and TEM. Moreover, improved wet transfer onto flat substrates decreased the sheet resistance of CVD-grown graphene films by a factor of 2, making them more suitable for device fabrication including transparent conductive films. These techniques increase the range of application of CVD-grown monolayer graphene.

METHODS

Dry Transfer to Wells. Large-area high-quality monolayer graphene was grown on 25 μm thick copper foils using a CVD method that we demonstrated recently.[14,59] PMMA powder (M_w 996 000, Sigma Aldrich) was dissolved in chlorobenzene (Sigma Aldrich). For 2 μm deep wells, PMMA solution (120 mg/mL) was spin-coated on graphene/copper foils at 4000 rpm for 30 s and dried in air. The PDMS block with a $\sim$1 cm diameter hole was gently pressed down onto the PMMA/graphene/copper. The copper was etched with ammonium persulfate (0.1 M) and dried in air after rinsing it with distilled water. The composite was placed on the target substrate having wells and heated at 180 °C for over 3 h. The PDMS block was peeled off while the sample was hot. The PMMA/graphene on substrate was annealed in a furnace with Ar ($\sim$500 sccm) and H$_2$ ($\sim$500 sccm) at 350 °C for $\sim$2 h to remove the PMMA. For 300 nm deep wells, PMMA solution (120 mg/mL) was spin-coated on graphene/copper foils at 1000 rpm for 30 s. The heat treatment was done at 150 °C for over 12 h.

Wet Transfer to Perforated Substrates. The PMMA solution (20 mg/mL) was spin-coated on graphene/copper foils at 4000 rpm for 30 s and dried in air. Ammonium persulfate (0.1 M, Sigma Aldrich) was used to etch copper, and the PMMA/graphene film was floated on the surface of the solution. The PMMA/graphene film was moved to distilled water several times to rinse the etchant residue. For a small hole substrate (2.7 μm diameter), silicon nitride supporting film TEM grid (Ted Pella) was used. A spacer (200 μm thick) was used to make the film flat. Water was pulled out with a syringe to lower the film onto the substrate while positioning the film with a needle. After drying it under vacuum for several hours, the sample was heated at 180 °C in air for over 30 min to enable the flattening of the graphene film. The PMMA was removed with an acetone bath, and the acetone was exchanged with ethanol and then HMDS. The sample was dried in air. To remove any PMMA residue, the grid was annealed in a furnace at 400 °C with Ar ($\sim$500 sccm) and H$_2$ ($\sim$500 sccm) for $\sim$1 h. A second type of substrate with larger holes ($\sim$10 μm diameter) was fabricated on a silicon substrate by deep silicon etching and KOH backside etching. For this case, the PMMA/graphene sample was directly annealed to remove the PMMA in a furnace at 400 °C with Ar ($\sim$500 sccm) and H$_2$ ($\sim$500 sccm) for $\sim$1 h, without using acetone.

Wet Transfer to Flat Substrates. The PMMA solution (20 mg/mL) was spin-coated on graphene/copper foils at 4000 rpm for 30 s and dried in air. The copper was etched with iron(III) nitrate solution (0.05 g/mL in water), and the PMMA/graphene film was floated on the surface of the solution. After rinsing the film with distilled water, the target substrate was placed in water with a tilting angle of $\sim$30° underneath the floating film. Water was pulled out with a syringe to lower the film onto the substrate while positioning the film with a needle. After drying it under vacuum for several hours, the sample was heated at 180 °C in air for over 30 min to enable the flattening of the graphene film. The PMMA was removed with an acetone bath. An additional annealing process can be performed at 400 °C with Ar ($\sim$500 sccm) and H$_2$ ($\sim$500 sccm) for $\sim$1 h to remove further residue.

Characterization. SEM images were taken with an FEI Quanta-600 FEG Environmental SEM. TEM images were taken with a JEOL 2010F. The sheet resistance and the optical transmittance were measured by the van der Pauw method (Keithley 6221 and 6514 instruments) and a spectroscopic ellipsometer system (JA Woolham M2000), respectively. A 514 nm excitation with a 100× objective (0.9 NA) and a 1800 line/mm grating was used for Raman spectroscopy of the graphene transferred to flat SiO$_2$ and the TEM grid. A 532 nm excitation laser with a 100× objective lens (WITec Alpha 300 micro-Raman imaging system) was used for Raman maps of the graphene transferred over depressions. AFM was performed by Park Scientific Instruments model CP using contact mode with 0.2 nN at a scanning speed of 0.5 Hz.

REFERENCES AND NOTES

1. May, J. W. Platinum Surface Leed Rings. *Surf. Sci.* **1969**, *17*, 267–270.
2. Blakely, J. M.; Kim, J. S.; Potter, H. C. Segregation of Carbon to (100) Surface of Nickel. *J. Appl. Phys.* **1970**, *41*, 2693–2697.
3. Eizenberg, M.; Blakely, J. M. Carbon Monolayer Phase Condensation on Ni(111). *Surf. Sci.* **1979**, *82*, 228–236.
4. Eizenberg, M.; Blakely, J. M. Carbon Interaction with Nickel Surfaces - Monolayer Formation and Structural Stability. *J. Chem. Phys.* **1979**, *71*, 3467–3477.
5. Dreyer, D. R.; Ruoff, R. S.; Bielawski, C. W. From Conception to Realization: An Historial Account of Graphene and Some Perspectives for Its Future. *Angew. Chem., Int. Ed.* **2010**, *49*, 9336–9344.
6. Zhang, Y. B.; Tan, Y. W.; Stormer, H. L.; Kim, P. Experimental Observation of the Quantum Hall Effect and Berry's Phase in Graphene. *Nature* **2005**, *438*, 201–204.
7. Zhu, Y. W.; Murali, S.; Cai, W. W.; Li, X. S.; Suk, J. W.; Potts, J. R.; Ruoff, R. S. Graphene and Graphene Oxide: Synthesis, Properties, and Applications. *Adv. Mater.* **2010**, *22*, 3906–3924.
8. Berger, C.; Song, Z. M.; Li, T. B.; Li, X. B.; Ogbazghi, A. Y.; Feng, R.; Dai, Z. T.; Marchenkov, A. N.; Conrad, E. H.; First, P. N.; *et al*. Ultrathin Epitaxial Graphite: 2D Electron Gas Properties and a Route toward Graphene-Based Nanoelectronics. *J. Phys. Chem. B* **2004**, *108*, 19912–19916.
9. Novoselov, K. S.; Geim, A. K.; Morozov, S. V.; Jiang, D.; Katsnelson, M. I.; Grigorieva, I. V.; Dubonos, S. V.; Firsov, A. A. Two-Dimensional Gas of Massless Dirac Fermions in Graphene. *Nature* **2005**, *438*, 197–200.
10. Lu, X. K.; Yu, M. F.; Huang, H.; Ruoff, R. S. Tailoring Graphite with the Goal of Achieving Single Sheets. *Nanotechnology* **1999**, *10*, 269–272.
11. Lu, X. K.; Huang, H.; Nemchuk, N.; Ruoff, R. S. Patterning of Highly Oriented Pyrolytic Graphite by Oxygen Plasma Etching. *Appl. Phys. Lett.* **1999**, *75*, 193–195.
12. Novoselov, K. S.; Geim, A. K.; Morozov, S. V.; Jiang, D.; Zhang, Y.; Dubonos, S. V.; Grigorieva, I. V.; Firsov, A. A. Electric Field Effect in Atomically Thin Carbon Films. *Science* **2004**, *306*, 666–669.
13. Yu, Q. K.; Lian, J.; Siriponglert, S.; Li, H.; Chen, Y. P.; Pei, S. S. Graphene Segregated on Ni Surfaces and Transferred to Insulators. *Appl. Phys. Lett.* **2008**, *93*, 113103.
14. Li, X. S.; Cai, W. W.; An, J.; Kim, S.; Nah, J.; Yang, D. X.; Piner, R.; Velamakanni, A.; Jung, I.; Tutuc, E.; *et al*. Large-Area Synthesis of High-Quality and Uniform Graphene Films on Copper Foils. *Science* **2009**, *324*, 1312–1314.
15. Li, X. S.; Magnuson, C. W.; Venugopal, A.; Tromp, R. M.; Hannon, J. B.; Vogel, E. M.; Colombo, L.; Ruoff, R. S. Large Area Graphene Single Crystals Grown by Low Pressure Chemical Vapor Deposition of Methane on Copper. *J. Am. Chem. Soc.* **2011**, *133*, 2816–2819.
16. Jiao, L. Y.; Fan, B.; Xian, X. J.; Wu, Z. Y.; Zhang, J.; Liu, Z. F. Creation of Nanostructures with Poly(methyl methacrylate)-Mediated Nanotransfer Printing. *J. Am. Chem. Soc.* **2008**, *130*, 12612–12613.
17. Reina, A.; Son, H. B.; Jiao, L. Y.; Fan, B.; Dresselhaus, M. S.; Liu, Z. F.; Kong, J. Transferring and Identification of Single- and Few-Layer Graphene on Arbitrary Substrates. *J. Phys. Chem. C* **2008**, *112*, 17741–17744.
18. Dean, C. R.; Young, A. F.; Meric, I.; Lee, C.; Wang, L.; Sorgenfrei, S.; Watanabe, K.; Taniguchi, T.; Kim, P.; Shepard, K. L.; *et al*. Boron Nitride Substrates for High-Quality Graphene Electronics. *Nat. Nanotechnol.* **2010**, *5*, 722–726.
19. Kim, K. S.; Zhao, Y.; Jang, H.; Lee, S. Y.; Kim, J. M.; Kim, K. S.; Ahn, J. H.; Kim, P.; Choi, J. Y.; Hong, B. H. Large-Scale Pattern Growth of Graphene Films for Stretchable Transparent Electrodes. *Nature* **2009**, *457*, 706–710.
20. Li, X. S.; Zhu, Y. W.; Cai, W. W.; Borysiak, M.; Han, B. Y.; Chen, D.; Piner, R. D.; Colombo, L.; Ruoff, R. S. Transfer of Large-Area Graphene Films for High-Performance Transparent Conductive Electrodes. *Nano Lett.* **2009**, *9*, 4359–4363.
21. Chen, J. H.; Jang, C.; Xiao, S. D.; Ishigami, M.; Fuhrer, M. S. Intrinsic and Extrinsic Performance Limits of Graphene Devices on SiO_2. *Nat. Nanotechnol.* **2008**, *3*, 206–209.
22. Booth, T. J.; Blake, P.; Nair, R. R.; Jiang, D.; Hill, E. W.; Bangert, U.; Bleloch, A.; Gass, M.; Novoselov, K. S.; Katsnelson, M. I.; *et al*. Macroscopic Graphene Membranes and Their Extraordinary Stiffness. *Nano Lett.* **2008**, *8*, 2442–2446.
23. Aleman, B.; Regan, W.; Aloni, S.; Altoe, V.; Alem, N.; Girit, C.; Geng, B. S.; Maserati, L.; Crommie, M.; Wang, F.; *et al*. Transfer-Free Batch Fabrication of Large-Area Suspended Graphene Membranes. *ACS Nano* **2010**, *4*, 4762–4768.
24. Kim, K.; Lee, Z.; Regan, W.; Kisielowski, C.; Crommie, M. F.; Zettl, A. Grain Boundary Mapping in Polycrystalline Graphene. *ACS Nano* **2011**, *5*, 2142–2146.
25. An, J.; Voelkl, E.; Suk, J. W.; Li, X. S.; Magnuson, C. W.; Fu, L. F.; Tiemeijer, P.; Bischoff, M.; Freitag, B.; Popova, E.; *et al*. Domain (Grain) Boundaries and Evidence of "Twinlike" Structures in Chemically Vapor Deposited Grown Graphene. *ACS Nano* **2011**, *5*, 2433–2439.
26. Huang, P. Y.; Ruiz-Vargas, C. S.; van der Zande, A. M.; Whitney, W. S.; Levendorf, M. P.; Kevek, J. W.; Garg, S.; Alden, J. S.; Hustedt, C. J.; Zhu, Y.; *et al*. Grains and Grain Boundaries in Single-Layer Graphene Atomic Patchwork Quilts. *Nature* **2011**, *469*, 389–392.
27. Cai, W. W.; Moore, A. L.; Zhu, Y. W.; Li, X. S.; Chen, S. S.; Shi, L.; Ruoff, R. S. Thermal Transport in Suspended and Supported Monolayer Graphene Grown by Chemical Vapor Deposition. *Nano Lett.* **2010**, *10*, 1645–1651.
28. Chen, S.; Moore, A. L.; Cai, W. W.; Suk, J. W.; An, J.; Mishra, C.; Amos, C.; Magnuson, C.; Kang, J.; Shi, L.; *et al*. Raman Measurements of Thermal Transport in Suspended Monolayer Graphene of Variable Sizes in Vacuum and Gaseous Environments. *ACS Nano* **2011**, *5*, 321–328.
29. Suk, J. W.; Piner, R. D.; An, J.; Ruoff, R. S. Mechanical Properties of Monolayer Graphene Oxide. *ACS Nano* **2010**, *4*, 6557–6564.
30. Nair, R. R.; Blake, P.; Grigorenko, A. N.; Novoselov, K. S.; Booth, T. J.; Stauber, T.; Peres, N. M. R.; Geim, A. K. Fine Structure Constant Defines Visual Transparency of Graphene. *Science* **2008**, *320*, 1308–1308.
31. Regan, W.; Alem, N.; Aleman, B.; Geng, B. S.; Girit, C.; Maserati, L.; Wang, F.; Crommie, M.; Zettl, A. A Direct Transfer of Layer-Area Graphene. *Appl. Phys. Lett.* **2010**, *96*, 113102.
32. Bunch, J. S.; Verbridge, S. S.; Alden, J. S.; van der Zande, A. M.; Parpia, J. M.; Craighead, H. G.; McEuen, P. L. Impermeable Atomic Membranes from Graphene Sheets. *Nano Lett.* **2008**, *8*, 2458–2462.
33. Lee, C.; Wei, X. D.; Kysar, J. W.; Hone, J. Measurement of the Elastic Properties and Intrinsic Strength of Monolayer Graphene. *Science* **2008**, *321*, 385–388.
34. Cha, M.; Shin, J.; Kim, J. H.; Kim, I.; Choi, J.; Lee, N.; Kim, B. G.; Lee, J. Biomolecular Detection with a Thin Membrane Transducer. *Lab Chip* **2008**, *8*, 932–937.
35. Unarunotai, S.; Murata, Y.; Chialvo, C. E.; Kim, H. S.; MacLaren, S.; Mason, N.; Petrov, I.; Rogers, J. A. Transfer of Graphene Layers Grown on SiC Wafers to Other Substrates and Their Integration into Field Effect Transistors. *Appl. Phys. Lett.* **2009**, *95*, 202101.
36. Caldwell, J. D.; Anderson, T. J.; Culbertson, J. C.; Jernigan, G. G.; Hobart, K. D.; Kub, F. J.; Tadjer, M. J.; Tedesco, J. L.; Hite, J. K.; Mastro, M. A.; *et al*. Technique for the Dry Transfer of Epitaxial Graphene onto Arbitrary Substrates. *ACS Nano* **2010**, *4*, 1108–1114.
37. Biedermann, L. B.; Beechem, T. E.; Ross, A. J.; Ohta, T.; Howell, S. W. Electrostatic Transfer of Patterned Epitaxial Graphene from SiC(0001) to Glass. *New J. Phys.* **2010**, *12*, 125016.
38. Allen, M. J.; Tung, V. C.; Gomez, L.; Xu, Z.; Chen, L. M.; Nelson, K. S.; Zhou, C. W.; Kaner, R. B.; Yang, Y. Soft Transfer Printing of Chemically Converted Graphene. *Adv. Mater.* **2009**, *21*, 2098–2102.

ARTICLE

39. Lee, D. H.; Kim, J. E.; Han, T. H.; Hwang, J. W.; Jeon, S.; Choi, S. Y.; Hong, S. H.; Lee, W. J.; Ruoff, R. S.; Kim, S. O. Versatile Carbon Hybrid Films Composed of Vertical Carbon Nanotubes Grown on Mechanically Compliant Graphene Films. *Adv. Mater.* **2010**, *22*, 1247–1252.

40. Hwang, J. O.; Lee, D. H.; Kim, J. Y.; Han, T. H.; Kim, B. H.; Park, M.; No, K.; Kim, S. O. Vertical ZnO Nanowires/Graphene Hybrids for Transparent and Flexible Field Emission. *J. Mater. Chem.* **2011**, *21*, 3432–3437.

41. Metzger, C.; Remi, S.; Liu, M. K.; Kusminskiy, S. V.; Neto, A. H. C.; Swan, A. K.; Goldberg, B. B. Biaxial Strain in Graphene Adhered to Shallow Depressions. *Nano Lett.* **2010**, *10*, 6–10.

42. Gomez-Navarro, C.; Burghard, M.; Kern, K. Elastic Properties of Chemically Derived Single Graphene Sheets. *Nano Lett.* **2008**, *8*, 2045–2049.

43. Chissoe, W. F.; Vezey, E. L.; Skvarla, J. J. Hexamethyldisilazane as a Drying Agent for Pollen Scanning Electron-Microscopy. *Biotech. Histochem.* **1994**, *69*, 192–198.

44. Ishigami, M.; Chen, J. H.; Cullen, W. G.; Fuhrer, M. S.; Williams, E. D. Atomic Structure of Graphene on SiO_2. *Nano Lett.* **2007**, *7*, 1643–1648.

45. van der Zande, A. M.; Barton, R. A.; Alden, J. S.; Ruiz-Vargas, C. S.; Whitney, W. S.; Pham, P. H. Q.; Park, J.; Parpia, J. M.; Craighead, H. G.; McEuen, P. L. Large-Scale Arrays of Single-Layer Graphene Resonators. *Nano Lett.* **2010**, *10*, 4869–4873.

46. Lazzeri, M.; Mauri, F. Nonadiabatic Kohn Anomaly in a Doped Graphene Monolayer. *Phys. Rev. Lett.* **2006**, *97*, 266407.

47. Ando, T. Anomaly of Optical Phonon in Monolayer Graphene. *J. Phys. Soc. Jpn.* **2006**, *75*, 124701.

48. Yan, J.; Zhang, Y. B.; Kim, P.; Pinczuk, A. Electric Field Effect Tuning of Electron-Phonon Coupling in Graphene. *Phys. Rev. Lett.* **2007**, *98*, 166802.

49. Das, A.; Pisana, S.; Chakraborty, B.; Piscanec, S.; Saha, S. K.; Waghmare, U. V.; Novoselov, K. S.; Krishnamurthy, H. R.; Geim, A. K.; Ferrari, A. C.; *et al.* Monitoring Dopants by Raman Scattering in an Electrochemically Top-Gated Graphene Transistor. *Nat. Nanotechnol.* **2008**, *3*, 210–215.

50. Ding, F.; Ji, H. X.; Chen, Y. H.; Herklotz, A.; Dorr, K.; Mei, Y. F.; Rastelli, A.; Schmidt, O. G. Stretchable Graphene: A Close Look at Fundamental Parameters through Biaxial Straining. *Nano Lett.* **2010**, *10*, 3453–3458.

51. Balandin, A. A.; Ghosh, S.; Bao, W. Z.; Calizo, I.; Teweldebrhan, D.; Miao, F.; Lau, C. N. Superior Thermal Conductivity of Single-Layer Graphene. *Nano Lett.* **2008**, *8*, 902–907.

52. Bonini, N.; Lazzeri, M.; Marzari, N.; Mauri, F. Phonon Anharmonicities in Graphite and Graphene. *Phys. Rev. Lett.* **2007**, *99*, 176802.

53. Mafra, D. L.; Samsonidze, G.; Malard, L. M.; Elias, D. C.; Brant, J. C.; Plentz, F.; Alves, E. S.; Pimenta, M. A. Determination of LA and TO Phonon Dispersion Relations of Graphene near the Dirac Point by Double Resonance Raman Scattering. *Phys. Rev. B* **2007**, *76*, 233407.

54. Basko, D. M.; Piscanec, S.; Ferrari, A. C. Electron-Electron Interactions and Doping Dependence of the Two-Phonon Raman Intensity in Graphene. *Phys. Rev. B* **2009**, *80*, 165413.

55. Casiraghi, C. Doping Dependence of the Raman Peaks Intensity of Graphene close to the Dirac Point. *Phys. Rev. B* **2009**, *80*, 2333407.

56. Cai, W. W.; Zhu, Y. W.; Li, X. S.; Piner, R. D.; Ruoff, R. S. Large Area Few-Layer Graphene/Graphite Films as Transparent Thin Conducting Electrodes. *Appl. Phys. Lett.* **2009**, *95*, 123115.

57. Gray, A.; Balooch, M.; Allegret, S.; De Gendt, S.; Wang, W. E. Optical Detection and Characterization of Graphene by Broadband Spectrophotornetry. *J. Appl. Phys.* **2008**, *104*, 053109.

58. Reina, A.; Jia, X. T.; Ho, J.; Nezich, D.; Son, H. B.; Bulovic, V.; Dresselhaus, M. S.; Kong, J. Large Area, Few-Layer Graphene Films on Arbitrary Substrates by Chemical Vapor Deposition. *Nano Lett.* **2009**, *9*, 3087–3087.

59. Li, X. S.; Magnuson, C. W.; Venugopal, A.; An, J.; Suk, J. W.; Han, B. Y.; Borysiak, M.; Cai, W. W.; Velamakanni, A.; Zhu, Y. W.; *et al.* Graphene Films with Large Domain Size by a Two-Step Chemical Vapor Deposition Process. *Nano Lett.* **2010**, *10*, 4328–4334.